Research in Astron. Astrophys. **2009** Vol. **9** No. **8**, 888 – 900
http://www.raa-journal.org *http://www.iop.org/journals/raa*

***R**esearch in*
***A**stronomy and*
***A**strophysics*

Applications of TP-AGB synthesis to Mira variables *

Chun-Hua Zhu[1,2], Guo-Liang Lü[1], Zhao-Jun Wang[1,2] and Jun Zhang[1]

[1] School of Physics, Xinjiang University, Urumqi 830046, China; *zhuchunhua@xju.edu.cn; zhj@xju.edu.cn*
[2] School of Science, Xi'an Jiaotong University, Xi'an 710049, China

Received 2008 December 27; accepted 2009 April 27

Abstract Employing recent TP-AGB synthesis, we have carried out a detailed study of Mira variables by means of a population synthesis code. We estimate that the total number of Mira variables in the Galaxy is from about 100 000 to 600 000 and their average lifetimes are between about 150 000 and 830 000 yr. The ratio of the number of O-Mira variables to that of C-Mira variables ranges from about 0.68 to 6.2. The effects of input physical parameters (mass loss rate, the minimum core mass for the third dredge-up, the third dredge-up efficiency and theoretical criterion for selecting Mira variables) on the Mira population are discussed.

Key words: stars: Mira variables — Galaxy: stellar content — stars: fundamental parameters

1 INTRODUCTION

Stars whose initial masses are between $0.9\,M_{\odot}$ and $8.0\,M_{\odot}$ go through an asymptotic giant branch (AGB) phase at the end of their life. As stars ascend along the AGB, it appears that they begin to pulsate when their effective temperatures drop below a certain level and the luminosities increase to a certain value. When the amplitude tends to increase with decreasing temperature and appreciable periodicity for stars in a high radial overtone drops gradually into a lower overtone, the stars approach the Mira stage (Percy 1997). At the top of the AGB, Mira variables (Miras) have carbon cores, surrounded by helium-rich layers, which in turn are surrounded by hydrogen-rich envelopes, and they are the coolest and the most luminous AGB stars. For Miras, detailed studies mainly focus on two aspects (Whitelock et al. 2007): i) the connection between mass loss and stellar parameters, such as stellar radius, stellar luminosity, etc.; ii) a period-luminosity relation between extreme luminosities and pulsation periods, giving Miras great potential as standard candles among old populations, which is very useful for galactic structure studies. In the past several decades, large numbers of observational data on Miras have been published, such as Feast et al. (1989), Hughes & Wood (1990), van Leeuwen et al. (1997), Feast & Whitelock (2000) and Menzies et al. (2006).

The general principle of AGB stellar evolution is well understood (Iben & Renzini 1983). However, due to extremely long CPU computing times, calculating full stellar evolution models of AGB stars is very difficult. Therefore, Iben & Truran (1978) first used synthetic evolution models for the AGB stars. According to the results in Iben & Truran (1978), Renzini & Voli (1981) used analytic algorithms to describe the evolution of the surface chemical abundances of intermediate-mass stars. Groenewegen & de Jong (1993) (hereafter GdJ93) showed a more realistic model for synthetic AGB

* Supported by the National Natural Science Foundation of China.

evolution in which the variation of the luminosity during the interpulse period and the effect of hot bottom burning (HBB) were included. Considering the rapid luminosity variations during a thermal pulse, Wagenhuber & Groenewegen (1998) (hereafter WG98) provided a fully updated and improved set of relations with respect to GdJ93. Karakas et al. (2002) (hereafter K02) showed the dependence of evolutionary behavior (such as the dredge-up law) on the various stellar parameters. Combining the treatment of dredge-up and HBB in GdJ93 and WG98 with the results in K02, Izzard et al. (2004) (hereafter I04) gave a new synthetic model for AGB stars. According to the analytical relations (WG98, K02 and I04) and some significantly theoretical improvements on the AGB stars (such as molecular opacities, mass-loss rate and pulsation modes), Marigo & Girardi (2007) updated the synthetic AGB models.

Therefore, it is possible to study Miras by theoretically synthetic models of AGB stars and understand some physical processes or constrain some physical parameters on the AGB phase by the observed properties of Miras. In the present paper, according to the recent synthetic models of AGBs (including GdJ93, WG98, K02, I04 and MG07), we simulate Miras (including their properties and some potentially observable parameters) in the Galaxy by using a Monte Carlo technique. By comparing simulated results with observational data of Miras, we give the effects of the mass loss rate, the third dredge-up (TDU) efficiency and the minimum core mass for TDU.

In Section 2, we present our assumptions and describe some details of the modeling algorithm. In Section 3, we discuss the main results. In Section 4, the main conclusions are given.

2 THE MODEL

2.1 Synthesis TP-AGB Evolution

Stellar evolution from the zero age main sequence up to the first thermal pulse is dealt with in the rapid evolution code of Hurley et al. (2000). After the first thermal pulse, we use a detailed synthetic model for thermal pulse AGB (TP-AGB).

2.1.1 Chemical abundance on the stellar surface

Based on observations, Miras can be divided into oxygen-rich Miras (O-Miras) and carbon-rich Miras (C-Miras) according to the ratio of the number of carbon atoms to that of oxygen atoms on the stellar surface which is denoted as C/O (Wood & Cahn 1977). The star is called an O-Mira if C/O in the stellar surface during the Mira phase is less than 1, or else is called a C-Mira. The chemical abundances on the stellar surface can be changed by three dredge-up processes and HBB. The initial abundances are taken from Anders & Grevesse (1989) for $Z = 0.02$. The following shows the initial abundances by mass fractions:

$$
\begin{array}{ll}
^{1}\mathrm{H}=0.68720; & ^{4}\mathrm{He}=0.29280; \\
^{12}\mathrm{C}=2.92293\times10^{-3}; & ^{13}\mathrm{C}=4.10800\times10^{-5}; \\
^{14}\mathrm{N}=8.97864\times10^{-4}; & ^{15}\mathrm{N}=4.14000\times10^{-6}; \\
^{16}\mathrm{O}=8.15085\times10^{-3}; & ^{17}\mathrm{O}=3.87600\times10^{-6}; \\
^{20}\mathrm{Ne}=2.29390\times10^{-3}; & ^{22}\mathrm{Ne}=1.45200\times10^{-4}.
\end{array}
$$

When stars ascend along the first giant branch, they will undergo first dredge-up. The stars whose core mass at the start of the early AGB is more massive than $0.8\,M_{\odot}$ will experience second dredge-up. Following Renzini & Voli (1981) and GdJ93, I04 gave a better analysis formula for the changes of chemical abundances on the stellar surface with an extension to include the minority species. In this work, we use the formula in I04 for the first and second dredge-ups. According to the synthesis model for TDU and HBB in I04 and GdJ93, Lü et al. (2008) and Zhu et al. (2008) simulate the evolution of chemical abundances on the stellar surface during the TP-AGB phase. In this work, we use their model. All details can be seen in Lü et al. (2008) and Zhu et al. (2008). In the following several subsections, we show the synthesis model of TP-AGB evolution in this work.

2.1.2 Core mass at the first thermal pulse

By using the rapid evolution code of Hurley et al. (2000), we can obtain the stellar mass ($M_{1\rm TP}$) and radius at the first thermal pulse. The core mass at the first thermal pulse, $M_{\rm c,1TP}$, is taken from K02:

$$M_{\rm c,1TP} = [-p_1(M_0 - p_2) + p_3]f + (p_4 M_0 + p_5)(1 - f)\,, \tag{1}$$

where $f = (1 + e^{(\frac{M_0 - p_6}{p_7})})^{-1}$ and the coefficients are seen in table 6 of K02, and M_0 is the initial mass in solar units.

2.1.3 Luminosity, radius, interpulse period and evolution of the core mass

We use the prescriptions of I04. The luminosity L and radius R are taken from equations (29) and (35) in I04, respectively . The radius and luminosity satisfy $L = 4\pi\sigma R^2 T_{\rm eff}^4$, where σ is the Stefan-Boltzmann constant and $T_{\rm eff}$ is the effective temperature of the star. The interpulse period $\tau_{\rm ip}$ marks the duration of a thermal pulse, and $\tau_{\rm ip}$ is:

$$\log_{10}(\tau_{\rm ip}/{\rm yr}) = a_{28}(M_{\rm c}/M_\odot - b_{28}) - 10^{c_{28}} - 10^{d_{28}} + 0.15\lambda^2, \tag{2}$$

where $M_{\rm c}$ is the core mass and the TDU efficiency λ is defined in Subsection 2.1.4. The coefficients are

$$\begin{aligned} a_{28} &= -3.821, \\ b_{28} &= 1.8926, \\ c_{28} &= -2.080 - 0.353Z + 0.200(M_{\rm env}/M_\odot + \alpha - 1.5), \\ d_{28} &= -0.626 - 70.30(M_{\rm c,1TP}/M_\odot - \zeta)(\Delta M_{\rm c}/M_\odot), \end{aligned}$$

where $M_{\rm env}$ represents the envelope mass, α is the mixing length parameter and equals to 1.75, $\zeta = \log(Z/0.02)$, and $\Delta M_{\rm c}$ is the change in core mass defined by $\Delta M_{\rm c} = M_{\rm c} - M_{\rm c,1TP}$.

2.1.4 The minimum core mass for TDU and TDU efficiency

TDU can only occur for stars with core masses larger than a certain core mass $M_{\rm c}^{\rm min}$. GdJ93 took $M_{\rm c}^{\rm min}$ as a constant 0.58 $M_\odot$. K02 found that $M_{\rm c}^{\rm min}$ depends on stellar mass and metallicity and gave a fitting formula by

$$M_{\rm c}^{\rm min} = a_1 + a_2 M_0 + a_3 M_0^2 + a_4 M_0^3\,, \tag{3}$$

where coefficients are shown in table 7 of K02. Based on the observed carbon star luminosity function of the Magellanic clouds, MG07 considered that the predicted $M_{\rm c}^{\rm min}$ by K02 is higher and $M_{\rm c}^{\rm min}$ of K02 must be decreased by an amount $\Delta M_{\rm c}^{\rm min}$ which depends on metallicity

$$\Delta M_{\rm c}^{\rm min} = \max[0.1, 0.1 - 100(Z - 0.008)]\,. \tag{4}$$

In this work, we carry out a series of numerical simulations (see Table 1):
(i) Like GDJ93, $M_{\rm c}^{\rm min}$=0.58 $M_\odot$;
(ii) Following K02, we take Equation (3) as $M_{\rm c}^{\rm min}$;
(iii) $M_{\rm c}^{\rm min} = {\rm Equation\ (3)} - {\rm Equation\ (4)}$.

In MG07, the correction for overshooting was considered so that their result approximates that of K02. In order to include an extreme $M_{\rm c}^{\rm min}$, we do not consider the correction for overshooting.

If $M_{\rm c}^{\rm min} < M_{\rm c,1TP}$, TDU can occur provided that stars enter the TP-AGB phase. Therefore, we take $M_{\rm c}^{\rm min}$=$M_{\rm c,1TP}$ if $M_{\rm c}^{\rm min} < M_{\rm c,1TP}$. Figure 1 shows different $M_{\rm c}^{\rm min}$ values in our simulations.

The TDU efficiency is defined by $\lambda = \frac{\Delta M_{\rm dred}}{\Delta M_{\rm c}}$ where $\Delta M_{\rm dred}$ is the mass brought up to the stellar surface during a thermal pulse. λ is a very uncertain parameter. K02 showed a relation of λ:

$$\lambda(N) = \lambda_{\rm max}[1 - \exp(-N/N_{\rm r})]\,, \tag{5}$$

Table 1 Parameters of the Synthetic Models of TP-AGB for the Population of Miras

Case	Mass loss rate	TDU efficiency λ	$M_{\rm c}^{\rm min}$
Case 1	Eq.(8)	Eq.(5)	$M_{\rm c}^{\rm min} = 0.58\,M_{\odot}$
Case 2	Eq.(7)($\eta = 1.5$)	Eq.(5)	$M_{\rm c}^{\rm min} = 0.58\,M_{\odot}$
Case 3	Eq.(11)	Eq.(5)	$M_{\rm c}^{\rm min} = 0.58\,M_{\odot}$
Case 4	Eq.(8)	Eq.(5)	Eq.(3)
Case 5	Eq.(8)	Eq.(5)	Eq.(3)–Eq.(4)
Case 6	Eq.(8)	$\lambda_{\rm max} = \max\{0.5, {\rm Eq.}(6)\}$	$M_{\rm c}^{\rm min} = 0.58\,M_{\odot}$
Case 7	Eq.(8)	$\lambda_{\rm max} = \max\{0.9, {\rm Eq.}(6)\}$	$M_{\rm c}^{\rm min} = 0.58\,M_{\odot}$
Case 8	Eq.(8)	$\lambda = 0.5$	$M_{\rm c}^{\rm min} = 0.58\,M_{\odot}$
Case 9	Eq.(8)	$\lambda = 0.75$	$M_{\rm c}^{\rm min} = 0.58\,M_{\odot}$

The mass loss rate, TDU efficiency λ, the maximum TDU efficiency $\lambda_{\rm max}$ and the minimum TDU core mass $M_{\rm c}^{\rm min}$ can be seen in Sect. 2.1.5 and Sect. 2.1.4. In cases 6 and 7, λ=Eq. (5), while $\lambda_{\rm max} = \max\{0.5, {\rm Eq.}\ (6)\}$ and $\max\{0.9, {\rm Eq.}\ (6)\}$, respectively.

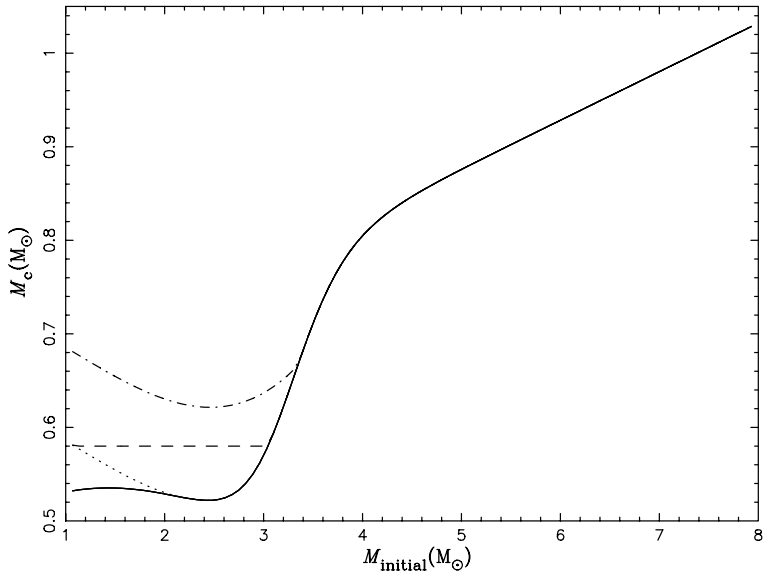

Fig. 1 Stellar initial mass vs. the core mass at the first thermal pulse $M_{\rm c,1TP}$ and the minimum core mass for TDU $M_{\rm c}^{\rm min}$. Solid line represents $M_{\rm c,1TP}$. Dashed, dot-dashed and dotted lines show $M_{\rm c}^{\rm min}$=0.58 $M_{\odot}$, Eq. (3) and Eqs. (3)–(4), respectively.

where λ increases gradually towards an asymptotic $\lambda_{\rm max}$ with N (the progressive number of thermal pulsations) increasing. $N_{\rm r}$ is taken from equation (6) in MG07 which reproduces the results for $N_{\rm r}$ in table 5 of K02. $\lambda_{\rm max}$ is given by (see eq. (6) in K02):

$$\lambda_{\rm max} = \frac{b_1 + b_2 M_0 + b_3 M_0^3}{1 + b_4 M_0^3}\,, \tag{6}$$

where coefficients are shown in table 8 of K02.

In the present paper, we carry out different numerical simulations for λ and $\lambda_{\rm max}$ (see Table 1).

2.1.5 Mass loss

During the TP-AGB phase, the star experiences significant mass loss whose mechanism is unknown. Mass loss has effects on the evolution of the AGB star including stellar final mass and chemical yield (Stancliffe & Jeffery 2007). We run several simulations by different mass loss rates.

Up to the first thermal pulse, the mass loss rates are given by Reimers' formula (Reimers 1975):

$$\dot{M} = -4.0 \times 10^{-13} \eta \frac{LR}{M} \, M_{\odot} \, \mathrm{yr}^{-1} \, , \tag{7}$$

where L, R and M are the stellar luminosity, radius, and mass, respectively, in solar units and the free parameter $\eta = 0.5$. During the TP-AGB phase, the following mass loss rates are used in different cases:

(i) Vassiliadis & Wood (1993) suggested a mass loss relation based on observations by

$$\log_{10}(\dot{M}) = \, -11.4 + 0.0123(P_0 - 100 \max(M/M_{\odot} - 2.5, 0.0)) \, , \tag{8}$$

where P_0 is the Mira pulsation period in days given by

$$\log_{10}(P_0) = \, -2.07 + 1.94 \log_{10}(R/R_{\odot}) - 0.90 \log_{10}(M/M_{\odot}) \, . \tag{9}$$

When $P_0 \geq 500$ d, the steady super-wind phase is modeled by the law

$$\dot{M}(M_{\odot} \, \mathrm{yr}^{-1}) = 2.06 \times 10^{-8} \frac{L/L_{\odot}}{v_{\infty}} \, , \tag{10}$$

where v_{∞} is the terminal velocity of the super-wind in km s^{-1}; we use $v_{\infty} = 15$ km s^{-1} in this paper.

(ii) We still use Reimers' formula but $\eta = 1.5$ for TP-AGB stars.

(iii) Based on the simulations of shock-driven winds in the atmospheres of Mira-like stars (Bowen 1988), Blöcker (1995) gave a mass loss rate similar to Reimers' formula

$$\dot{M} = 4.83 \times 10^{-9} M^{-2.1} L^{2.7} \dot{M}_{\mathrm{Reimers}} \, , \tag{11}$$

where $\dot{M}_{\mathrm{Reimers}}$ is given by Equation (7) but $\eta = 0.02$ (Stancliffe & Jeffery 2007) .

2.2 Miras' Positions in Hertzsprung-Russell (HR) Diagram

It is unknown when an AGB star becomes a Mira. In the present paper, we use the following two criteria for Miras:

(i) The Miras appear in a limited region in the HR diagram. According to observational data, Groenewegen & de Jong (1994) and Gautschy (1999) discussed this region. The most widely used definition that attempts to determine the region in the HR diagram where stars become Miras is the work of Gautschy (1999). Following Gautschy (1999), we assume that stars are Miras if their effective temperatures T_{eff} are lower than $10^{3.49}$ K and their luminosities are higher than $10^{3.25} \, L_{\odot}$ (also see Zhu & Zha 2005, Ferrarotti & Gail 2006 and Lü et al. 2007).

(ii) In regards to the pulsation mode of Miras, which are either the fundamental mode or the first overtone pulsator, it is very controversial (e.g. Wood & Sebo 1996; Feast 1996; Hofmann et al. 2002). MG07 believed that all stars start their AGB evolution as first overtone pulsators, and the transition from the first overtone to the fundamental mode pulsation may take place when a minimum luminosity L_{1-0} is reached. We assume that the stars evolve into Miras when their luminosities are higher than L_{1-0}. Using the results of the pulsation models in Ostlie & Cox (1986), MG07 gave a good fitting relation by:

$$\log L_{1-0}/L_{\odot} = \, -14.516 + 2.277 \log M/M_{\odot} + 5.046 \log T_{\mathrm{eff}} - 0.084 \log(Z/0.02). \tag{12}$$

In our simulations, the Miras selected by criterion (i) and criterion (ii) are simply noted as Miras$^{(\mathrm{i})}$ and Miras$^{(\mathrm{ii})}$, respectively.

2.3 Basic Parameters of the Monte Carlo Simulation

For the population synthesis of single stars, the main input parameters of the model are: (i) the initial mass function (IMF); (ii) the lower and upper mass cut-offs $M_{\rm l}$ and $M_{\rm u}$ to the initial mass function; (iii) the relative age of the single stellar population; (iv) the metallicity Z of the star.

A simple approximation to the IMF in Miller & Scalo (1979) is used. The stellar mass is generated using the formula suggested by Eggleton et al. (1989)

$$M_{\rm initial} = \frac{0.19X}{(1-X)^{0.75} + 0.032(1-X)^{0.25}}\,, \tag{13}$$

where X is a random variable uniformly distributed in the range [0,1], and $M_{\rm initial}$ is the stellar mass from $0.8\,M_{\odot}$ to $8\,M_{\odot}$.

This work attempts to simulate Miras in the Galactic disk. Z is taken as 0.02. We take 1×10^6 stars for each simulation. To calculate the average lifetime and number of Miras, we assume that one star with $M_{\rm initial} \geq 0.8\,M_{\odot}$ is formed annually in the Galactic disk (Yungelson & Tutukov 1993; Han et al. 1995; Lü et al. 2006).

3 RESULTS

We construct a set of models in which we vary different input parameters relevant to Miras. Table 1 lists all cases considered in the present work.

3.1 Lifetime and Number of Miras

First, we discuss the gross properties of the modeled population of Miras and then proceed to the more detailed comparison of the influence of different assumptions. As Table 2 shows, the numbers of Miras$^{\rm (i)}$ in the Galaxy may range from 1.01×10^5 (case 4) to 2.23×10^5 (case 2). Their average lifetimes are from 1.47×10^5 yr (case 4) to 4.02×10^5 yr (case 2). In Table 3, the numbers of Miras$^{\rm (ii)}$ in the Galaxy are from about 4.31×10^5 (cases 4 and 8) to 5.90×10^5 (case 7), and their average lifetimes are between about 6.05×10^5 yr (cases 4 and 8) and 8.28×10^5 yr (case 7). The average lifetimes of Miras$^{\rm (ii)}$ are about 1.7 (case 2) to 4.1 (case 4) times of those of Miras$^{\rm (i)}$, and the numbers of Miras$^{\rm (ii)}$ are about 2.0 (case 2) to 4.3 (case 4) times of those of Miras$^{\rm (i)}$. The main reason is shown in Figure 2. For the stars with masses larger than $5\,M_{\odot}$, they enter the Mira phase earlier under criterion (ii) than under criterion (i).

Table 2 Different Models of Miras$^{\rm (i)}$ Population

Case	Miras$^{\rm (i)}$		O-Miras$^{\rm (i)}$		C-Miras$^{\rm (i)}$		O-Miras$^{\rm (i)}$ ($P_0 > 500$ d)		C-Miras$^{\rm (i)}$ ($P_0 > 500$ d)	
	Lifetime 10^5 yr	Number 10^4	Lifetime 10^5 yr	Number 10^4	Lifetime 10^5 yr	Number 10^4	Lifetime 10^5 yr	Number 10^4	Lifetime 10^5 yr	Number 10^4
(1)	(2)	(3)	(4)	(5)	(6)	(7)	(8)	(9)	(10)	(11)
Case 1	1.59	11.0	1.59	8.14	1.36	2.81	0.63	2.50	1.24	2.55
Case 2	4.02	22.3	3.09	13.3	4.13	9.08	2.46	8.72	3.31	7.27
Case 3	2.56	17.8	2.23	11.9	2.60	5.96	1.10	4.79	1.98	4.53
Case 4	1.47	10.1	1.56	8.70	0.96	1.40	0.62	2.65	1.69	2.47
Case 5	1.65	11.3	1.54	7.29	1.69	4.03	0.66	2.35	1.11	2.65
Case 6	1.68	11.5	1.59	7.95	1.35	3.57	0.64	2.28	1.04	2.77
Case 7	2.30	15.8	1.47	6.38	2.86	9.44	0.73	2.01	0.84	2.78
Case 8	1.67	11.4	1.51	7.45	1.40	3.99	0.48	1.60	0.88	2.53
Case 9	2.04	14.0	1.45	6.29	2.31	7.69	0.53	1.46	0.79	2.65

The first column gives case number according to Table 1. Cols. (2), (4), (6), (8) and (10) give the lifetimes of Miras, O-Miras, C-Miras, O-Miras with $P_0 > 500$ d and C-Miras with $P_0 > 500$ d, respectively. Cols. (3), (5), (7), (9) and (11) show the numbers of Miras, O-Miras, C-Miras, O-Miras with $P_0 > 500$ d and C-Miras with $P_0 > 500$ d in the Galaxy, respectively.

Table 3 Same as in Table 2, but for Miras$^{(ii)}$

Case	Miras$^{(ii)}$		O-Miras$^{(ii)}$		C-Miras$^{(ii)}$		O-Miras$^{(ii)}$ ($P_0 > 500$ d)		C-Miras$^{(ii)}$ ($P_0 > 500$ d)	
	Lifetime 10^5 yr	Number 10^4	Lifetime 10^5 yr	Number 10^4	Lifetime 10^5 yr	Number 10^4	Lifetime 10^5 yr	Number 10^4	Lifetime 10^5 yr	Number 10^4
(1)	(2)	(3)	(4)	(5)	(6)	(7)	(8)	(9)	(10)	(11)
Case 1	6.48	46.2	5.67	33.1	6.34	13.1	0.37	1.48	0.66	1.36
Case 2	6.91	43.8	5.50	31.2	5.73	12.6	2.30	7.72	3.11	6.83
Case 3	6.55	47.1	5.90	35.6	5.02	11.5	1.02	4.31	1.87	4.27
Case 4	6.05	43.1	5.60	35.0	5.59	8.14	0.40	1.82	0.79	1.14
Case 5	6.66	47.5	5.63	30.5	7.08	17.0	0.36	1.32	0.61	1.46
Case 6	6.62	47.2	5.70	33.3	5.25	13.9	0.35	1.25	0.60	1.58
Case 7	8.28	59.0	5.43	30.2	8.72	28.8	0.36	1.00	0.49	1.60
Case 8	6.05	43.1	5.27	32.3	3.76	10.8	0.35	1.18	0.57	1.63
Case 9	7.28	51.9	5.27	29.6	6.67	22.3	0.36	1.00	0.52	1.71

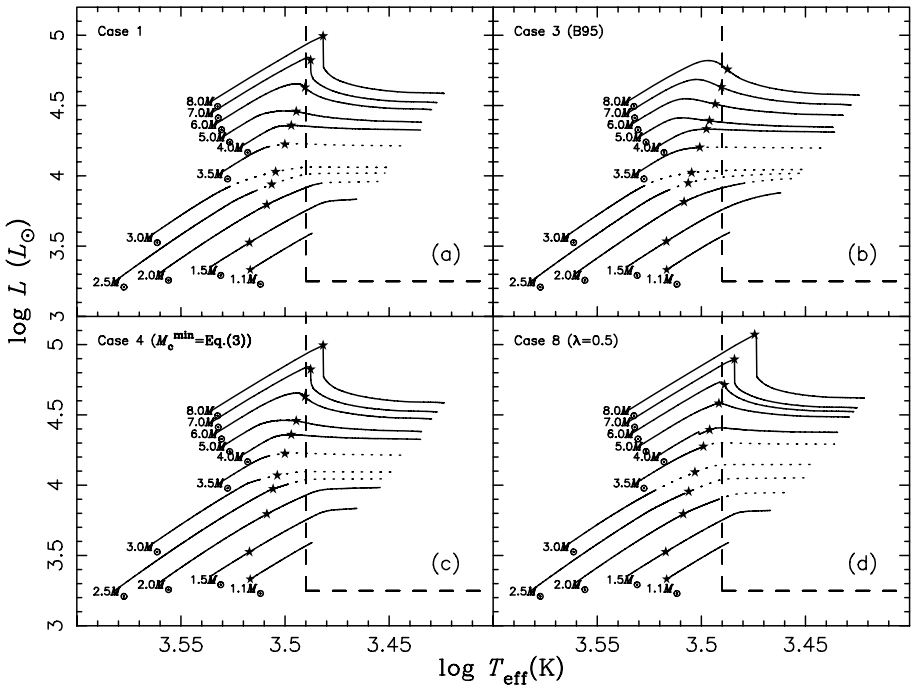

Fig. 2 Position of TP-AGB stars and Miras in the HR diagram for different cases. The solid lines mean O-rich TP-AGB stars and dotted lines represent C-rich TP-AGB stars. The symbols '⋆' show where the stellar luminosities are just higher than L_{1-0} (see Sect. 2.2). The regions surrounded by dashed lines show the position of Miras in the HR diagram based on criterion (i) (see Sect. 2.2). Stellar initial masses are shown by the side of lines.

Ignoring mass loss, Wood & Cahn (1977) estimated Mira lifetimes of about 4×10^5 yr, which is consistent with ours. The average lifetime of a Mira estimated by observations is about 6×10^4 yr (Wood 1990). Our results are about $2.5 - 12$ times longer than the observations. The main reason originates from mass loss. From case 1 to cases 2 and 3, it is obvious that the Mira lifetime depends strongly on mass loss. As Wood (1990) mentioned, the mass loss rates in the theoretical lifetime are not sufficiently high. Therefore, we overestimate the lifetimes and numbers of Miras in this work.

For Miras$^{(i)}$, the average lifetimes of O-Miras$^{(i)}$ and C-Miras$^{(i)}$ are from 1.45×10^5 yr (case 9) to 3.09×10^5 yr (case 2) and from 9.6×10^4 yr (case 4) to 4.13×10^5 yr (case 2), respectively. The ranges of their numbers in the Galaxy are from 6.29×10^4 (case 9) to 1.33×10^5 (case 2) for O-Miras$^{(i)}$ and from 1.40×10^4 (case 4) to 9.44×10^4 (case 7) for C-Miras$^{(i)}$. The ratios of the number of O-Miras$^{(i)}$ to that of C-Miras$^{(i)}$ range from about 0.68 (case 7) to 6.2 (case 4). For Miras$^{(ii)}$, the average lifetimes of O-Miras$^{(ii)}$ and C-Miras$^{(ii)}$ are from 5.27×10^5 yr (cases 8 and 9) to 5.90×10^5 yr (case 3) and from 3.76×10^5 yr (case 8) to 8.72×10^5 yr (case 7), respectively. The ranges of their numbers in the Galaxy are from 2.96×10^5 (case 9) to 3.56×10^5 (case 3) for O-Miras$^{(ii)}$ and from 8.14×10^4 (case 4) to 2.88×10^5 (case 7) for C-Miras$^{(ii)}$. The ratios of the number of O-Miras$^{(ii)}$ to that of C-Miras$^{(ii)}$ range from about 1.32 (case 7) to 4.3 (case 4).

For an optically selected sample, Wood & Cahn (1977) found that the number ratio of O-Miras to that of C-Miras is about 14, which is higher than ours. According to Ferrarotti & Gail (2006), when stars have high enough mass loss rate and low effective temperature, they produce dust. In general, C-Miras have lower effective temperature and higher mass loss rate than O-Miras (see Fig. 2). It is easier for C-Miras to produce thick dust shells than O-Miras, therefore it is more difficult for C-Miras to be detected in the optical spectrum. The result in Wood & Cahn (1977) may be biased. Olivier et al. (2001) showed that dust enshrouding Miras are biased to long period stars and the ratio of O-Miras to C-Miras with thick dust shells is about 1. Ferrarotti & Gail (2006) found a critical period $P \approx 500$ d at which a star transits from a visible Mira to one with massive thick dust shells. In our simulations, the number ratios of O-Miras$^{(i)}$ to C-Miras$^{(i)}$ with $P_0 >$500 d are from about 0.55 (case 9) to 1.19 (case 2). The ratios for Miras$^{(ii)}$ are from 0.58 (case 9) to 1.60 (case 4). Our result is consistent with observations. From the number ratios of O-Miras to C-Miras with or without $P_0 >$500 d, one can find that the ratios are greatly determined by TDU efficiency λ which is affected by $M_{\rm c}^{\rm min}$ and $\lambda_{\rm max}$.

3.2 The Effects of Parameters

In this subsection, we discuss the effects of mass loss rate $M_{\rm c}^{\rm min}$, TDU efficiency λ and select several typical cases: cases 1, 3, 4 and 8. In the followings, cases 3, 4 and 8 are noted as case 3 (B95), case 4 ($M_{\rm c}^{\rm min} = $ Eq. (3)) and case 8 ($\lambda = 0.5$), respectively.

Position in the HR diagram: In Figure 2, the different evolutionary phases during TP-AGB in the HR diagram are given. For the stars whose initial masses are higher than 4 $M_\odot$, their luminosities have greatly protuberant curves which stem from HBB. The luminosity produced by HBB depends on the mass of the stellar envelope. After reaching a maximum, the total luminosity exhibits a final decline due to the decrease in the envelope's mass, and finally converges to the value predicted by the core mass-luminosity. In addition, no C-stars whose initial masses are higher than 4 $M_\odot$ result from HBB. For different mass loss rates (see panels (a) and (b) in Fig. 2), the mass loss rate in case 3 (B95) depends on the stellar luminosity more than that in case 1. Thus, the mass loss rate increases more rapidly with the increase of stellar luminosity, which results in a sharp decrease of stellar envelope mass, and then the extinguishing of HBB. So, the star cannot reach the maximum luminosity which it achieves in case 1.

As Equation (12) shows, the critical luminosity L_{1-0} depends on the stellar mass and effective temperature. For a given temperature, the lower the stellar mass is, the lower L_{1-0} is. Low mass stars satisfy criterion (ii) for earlier selecting Miras. For the stars with initial masses larger than 4 $M_\odot$, due to HBB, the luminosities rapidly are enhanced, and can reach L_{1-0} at their maximum.

Core mass: During the TP-AGB phase, the core mass evolution is very important because it determines stellar luminosity. In Figure 3, the core mass at the first thermal pulse and the final core mass at the end of TP-AGB are shown. Comparing with cases 1 and 3, mass loss rate in this work has no major effect on the core mass evolution of TP-AGB. As Figure 3 shows, case 8 gives the high final core mass due to a low TDU efficiency ($\lambda = 0.5$).

Variety of C/O: Figure 4 shows the varieties of C/O during the TP-AGB phase. It represents the changes of λ. In the panel (a) of Figure 4, for a star with initial mass 1.5 $M_\odot$, C/O changes in case 8 ($\lambda = 0.5$), while it does not change in cases 1 and 3 (B95) because $\lambda_{\rm max} \approx 0$ (see fig. 4 of K02), and does not change in case 4 ($M_{\rm c}^{\rm min} = $ Eq.(3)) because stellar core mass is less than $M_{\rm c}^{\rm min}$. In panel

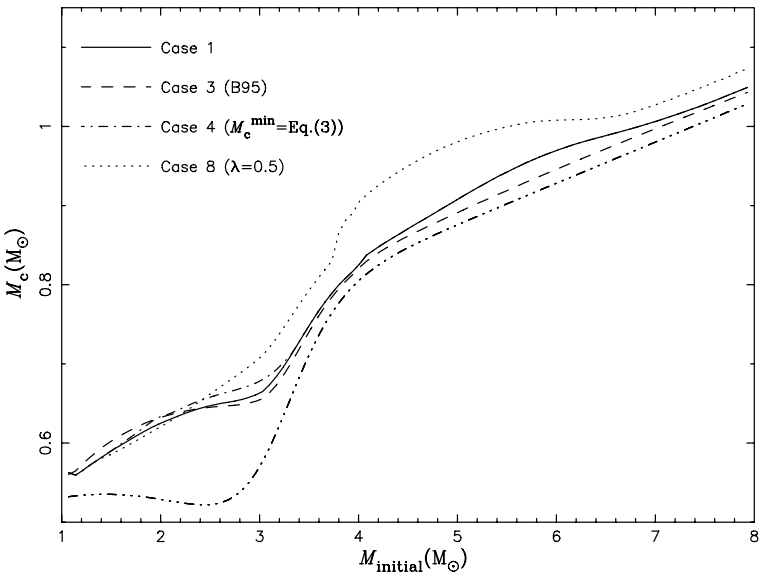

Fig. 3 Relation of the initial mass, the core mass at the first thermal pulse and the final core mass at the end of TP-AGB. The dotted-dotted-dotted-dashed line represents the core mass at the first thermal pulse (see Eq. (1)). The final core mass at the end of TP-AGB is shown by different style lines with corresponding cases represented in the upper left region.

(b) of Figure 4, for a star with initial mass $2.0\,M_\odot$, all of the C/Os change but the variety in case 4 ($M_{\rm c}^{\rm min}$ = Eq. (3)) is much smaller because of the high $M_{\rm c}^{\rm min}$. As panels (b) and (c) in Figure 4 show, TDU efficiencies, which are represented by the λs, have a strong effect on the variances of C/O. For a massive star with a mass larger than $4\,M_\odot$, due to HBB, C/O is almost a constant like that in panel (d) of Figure 4.

Lifetime: Figure 5 gives the stellar lifetimes in different evolutionary phases. The phases of C-stars, Miras$^{\rm (i)}$ and Miras$^{\rm (ii)}$ are a small fraction of the whole TP-AGB. For stars with lower masses, the lifetimes of Miras$^{\rm (ii)}$ are longer than those of Miras$^{\rm (i)}$, while they are similar for the stars with masses higher than $5\,M_\odot$. As Figure 5 shows, the mass loss rate, $M_{\rm c}^{\rm min}$ and λ can affect the duration of C-stars, Miras$^{\rm (i)}$ and Miras$^{\rm (ii)}$. In panels (a) and (b) of Figure 5, there are lower durations around initial mass $3\,M_\odot$ for C-stars, Miras$^{\rm (i)}$ and Miras$^{\rm (ii)}$. The main reason is the following: for a star with initial mass $3\,M_\odot$, due to $M_{\rm c}^{\rm min} \simeq M_{\rm c,1TP}$ when the star evolves into the TP-AGB phase (see Fig. 1), TDU with a high efficiency λ can occur. The increase of its core mass is slow so that it has remained unchanged a long time before it enters the C-star, Mira$^{\rm (i)}$ and Mira$^{\rm (ii)}$ phases.

According to the above discussions, we give the effects of input physical parameters:

Mass loss rate: The description of mass loss can be seen in Section 2.1.5. The mass loss rate of Equation (8) obviously depends on the stellar pulsational period. The mass loss rate of Equation (11) depends on the luminosity more than that of Equation (11). A high mass loss rate during the Mira phase results in a quick decrease of the stellar envelope mass. Then, the duration of Miras will shorten. For Miras$^{\rm (i)}$, stars have entered the later phase of the AGB and generally have long pulsational periods. The average mass loss rate of Equation (8) during the Mira$^{\rm (i)}$ phase is higher than that of Equations (7) and (11). The average lifetime of Miras$^{\rm (i)}$ in case 1 is shorter and the number is smaller than those in cases 2 and 3. However, for Miras$^{\rm (ii)}$, stars still stay in the early phase of the AGB, and have short pulsational periods and low luminosity. Therefore, the average mass loss rate of Equation (7) during its Mira$^{\rm (ii)}$ phase is higher than those of Equations (8) and (11). Willson gave a detailed description of $\mathrm{d}(\log \dot{M})/\mathrm{d}(\log L)$ for the above three mass loss laws (see fig. 1 in Willson (2007)). For the average

lifetime and the number of Miras in the Galaxy, the mass loss rate introduces an uncertainty up to a factor of about 3.

The minimum core mass for TDU $M_{\rm c}^{\rm min}$: $M_{\rm c}^{\rm min}$ determines the lowest initial mass for TDU and directly affects C/O changes of the low mass star. As Tables 2 and 3 show, the number of C-Miras [(i)] or

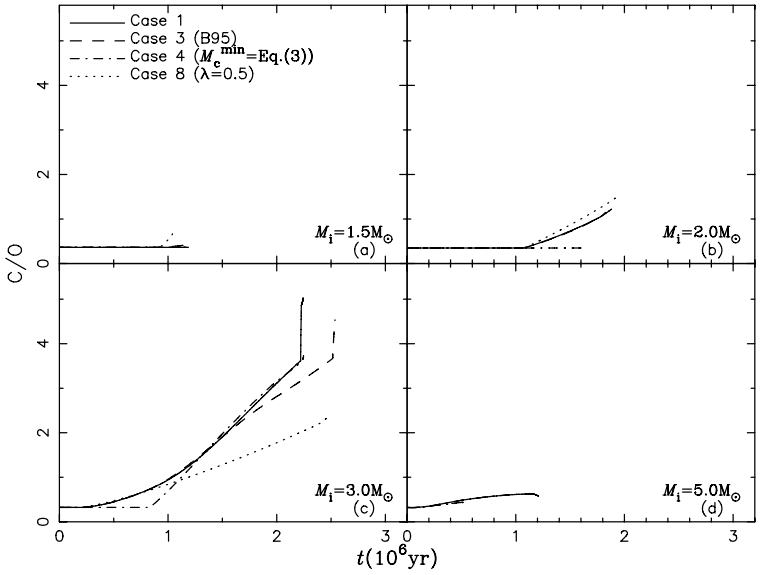

Fig. 4 Varieties of C/O during the TP-AGB phase in different cases and initial masses. Stellar initial masses are shown in the lower right corners. Different style lines with corresponding cases are shown in the upper left region of Fig. 4(a).

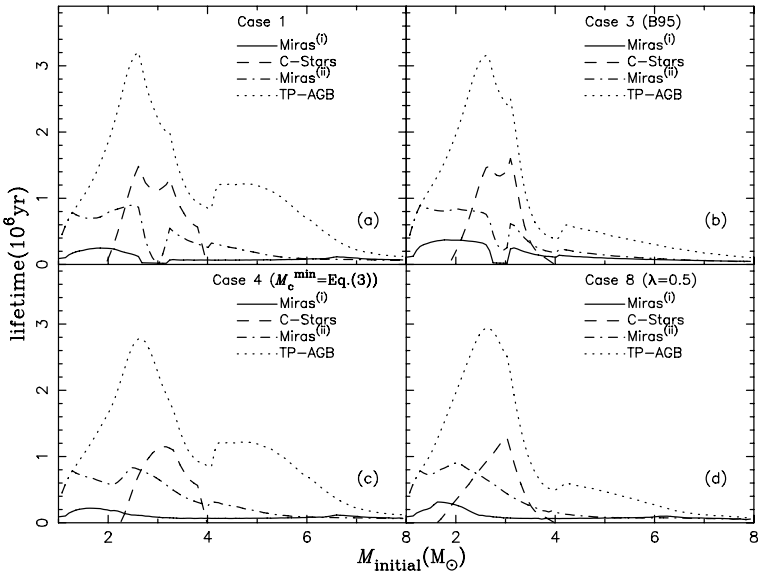

Fig. 5 Stellar lifetimes in different evolutionary phases. Different cases and style lines with their corresponding stellar evolutionary phases are represented in the upper right regions.

C-Miras$^{(ii)}$ is the least in case 4 which has the highest $M_{\rm c}^{\rm min}$ (see Fig. 1). $M_{\rm c}^{\rm min}$ has a great effect on the ratio of the number of O-Miras$^{(i)}$ or O-Miras$^{(ii)}$ to that of C-Miras$^{(i)}$ or C-Miras$^{(ii)}$ within a factor of about 3.

The TDU efficiency λ and $\lambda_{\rm max}$: Evolution of the chemical abundances on the stellar surface is greatly affected by $\lambda_{\rm max}$ and λ. The carbon abundance in the stellar surface depends on the TDU. Therefore, the TDU efficiency has a great effect on the formation of C-Miras. Compared with observational estimates, case 7 ($\lambda_{\rm max} = \max(0.9, {\rm Eq.}(6))$) and case 9 ($\lambda = 0.75$) result in too small a number ratio of O-Miras$^{(i)}$ to C-Miras$^{(i)}$ or O-Miras$^{(ii)}$ to C-Miras$^{(ii)}$. The physical parameters assumed in cases 7 and 9 are unsuitable. $\lambda_{\rm max}$ and λ greatly affect the ratio of the number of O-Miras$^{(i)}$ or O-Miras$^{(ii)}$ to that of C-Miras$^{(i)}$ or C-Miras$^{(ii)}$ up to a factor of about 4.

3.3 Mass Distributions of Miras

Figure 6 shows the number (all numbers are normalized to 1) distributions of modeled Galactic Miras as a function of the initial stellar mass. As panels (a) and (b) in Figure 6 show, the initial masses of the progenitors of Miras$^{(i)}$ and Miras$^{(ii)}$ are mainly between $1.0\,M_{\odot}$ and $2.0\,M_{\odot}$, which result from the IMF (see Eq.(13)) and the lifetimes of Miras$^{(i)}$ and Miras$^{(ii)}$. For the progenitors of C-Miras$^{(i)}$ and C-Miras$^{(ii)}$ in panels (c) and (d) of Figure 6, the ranges of initial masses are between $2.0\,M_{\odot}$ and $4.0\,M_{\odot}$, which are determined by $M_{\rm c}^{\rm min}$ and HBB. Comparing case 4 ($M_{\rm c}^{\rm min}$=Eq. (3)) and case 8 ($\lambda = 0.5$) in Figure 6(c) and 6(d), we can easily see the effects of the parameters $M_{\rm c}^{\rm min}$ and λ.

Figure 7 gives the mass distributions of modeled Galactic Miras as a function of the stellar mass. As panel (a) in Figure 7 shows, the masses of Miras$^{(i)}$ are almost always between $0.8\,M_{\odot}$ and $2.0\,M_{\odot}$ and their peak is at $1.7\,M_{\odot}$. For Miras$^{(ii)}$ in panel (b) of Figure 7, the majority of masses are from $0.8\,M_{\odot}$ to $3.5\,M_{\odot}$. The peak of the masses of C-Miras$^{(i)}$ in panel (c) of Figure 7 appears at $2.0\,M_{\odot}$ and the peak for C-Miras$^{(ii)}$ in panel (d) of Figure 7 is at $1.7\,M_{\odot}$.

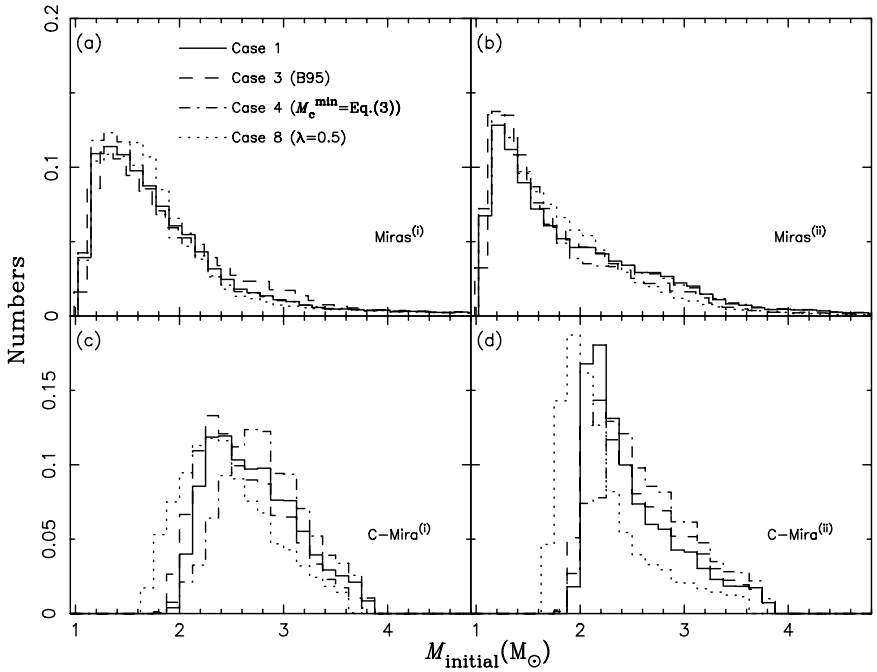

Fig. 6 Number (all numbers are normalized to 1) distributions of modeled Galactic Miras as a function of the initial stellar mass. The key to the line-styles representing different models is given in panel (a).

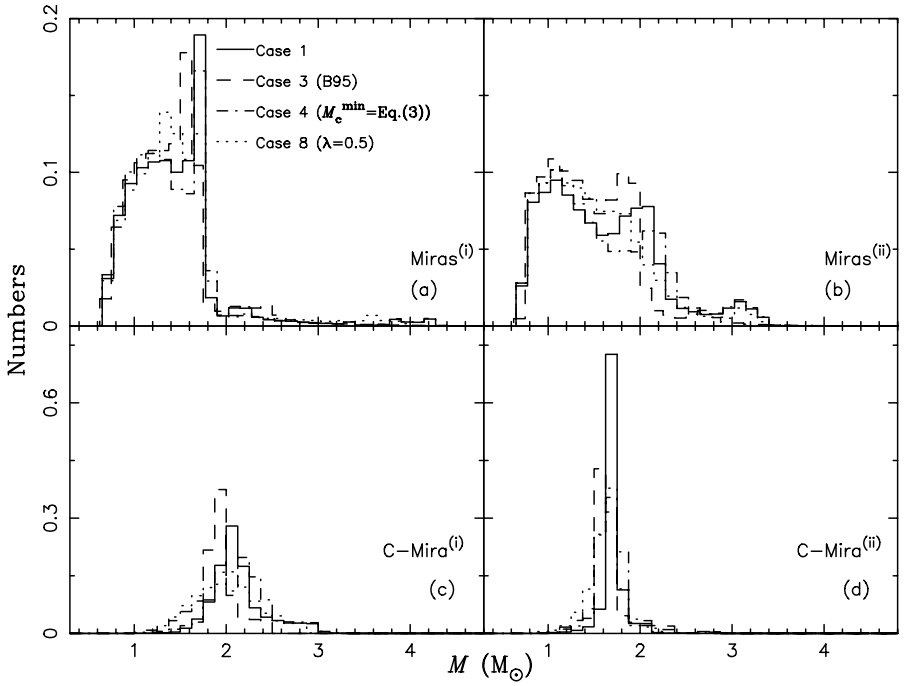

Fig. 7 Number (normalized to 1) distributions of modeled Galactic Miras as a function of the stellar mass. The key to the line-styles representing different models is given in panel (a).

4 CONCLUSIONS

Employing the population synthesis method, we perform a detailed study of Miras. Several important conclusions can be drawn:

(1) In the Galaxy, there are about 100 000 to 600 000 Miras and their lifetimes are between 150 000 and 830 000 yr. The ratio of the number of O-Miras to that of C-Miras ranges from 0.68 to 6.2.
(2) The mass loss rate has a great effect on the lifetimes of Miras, up to a factor of about 3. The ratio of the number of O-Miras to that of C-Miras is chiefly determined by $M_{\rm c}^{\rm min}$ (It introduces an uncertainty up to a factor of about 3) and λ (It introduces an uncertainty up to a factor of about 4). The theoretical criteria for selecting Miras are crucial for studying the population of Miras up to a factor of about 4 for their number and average lifetime.
(3) The ranges of the initial masses of the progenitors of Miras are mainly from about $1.0\,M_{\odot}$ to $2.0\,M_{\odot}$. The theoretical criteria for selecting Miras have a great effect on the distribution of C-Miras' masses. For C-Miras$^{(\rm i)}$ and C-Miras$^{(\rm ii)}$, the peaks are around $2.0\,M_{\odot}$ and $1.7\,M_{\odot}$, respectively.

Acknowledgements This work was funded by the National Natural Science Foundation of China (NSFC) under Nos. 10763001 and 10647003, the Natural Science Foundation of Xinjiang under No. 2009211B01 and the Scientific Research Program of the Higher Education Institution of Xinjiang under No. XJEDU2008S12.

References

Anders, E., & Grevesse, N. 1989, Grochim. Cosmochim. Acta, 53, 197
Blöcker, T. 1995, A&A, 297, 727
Bowen, G. H. 1988, ApJ, 329, 299
Eggleton, P. P., Fitechett, M. J., & Tout, C. A. 1989, ApJ, 347, 998
Feast, M. W., Glass, I. S., Whitelock, P. A., & Catchpole, R. M. 1989, MNRAS, 241, 375
Feast, M. W. 1996, MNRAS, 278, 11
Feast, M. W., & Whitelock, P. A. 2000, MNRAS, 317, 460
Ferrarotti, A. S., & Gail, H. P. 2006, A&A, 447, 553
Gautschy, A. 1999, A&A, 349, 209
Groenewegen, M. A. T., & de Jong, T. 1993, A&A, 267, 410 (GdJ93)
Groenewegen, M. A. T., & de Jong, T. 1994, A&A, 283, 463
Han, Z., Eggleton, P. P., Podsiadlowski, P., & Tout, C. A. 1995, MNRAS, 277, 1443
Hofmann, K. H., et. al. 2002, New Astronomy, 7, 9
Hughes, S. M. G., & Wood, P. R. 1990, AJ, 99, 784
Hurley, J. R., Pols, O. R., & Tout, C. A. 2000, MNRAS, 315, 543 (H00)
Iben, I. Jr., & Renzini, A. 1983, ARA&A, 21, 271
Iben, I. Jr., & Truran, J. W. 1978, ApJ, 220, 980
Izzard, R. G., Tout, C. A., Karakas, A. I., & Pols, O. R. 2004, MNRAS, 350, 407 (I04)
Karakas, A. I., Lattanzio, J. C., & Pols, O. R. 2002, Publ. Astron. Soc. Aust., 19, 515 (K02)
Lü, G. L., Yungelson, L., & Han, Z. 2006, MNRAS, 372, 1389
Lü, G. L., Zhu, C. H., & Han, Z. 2007, ChJAA (Chin. J. Astron. Astrophys.), 7, 101
Lü, G. L., Zhu, C. H., Han, Z., & Wang, Z. J. 2008, ApJ, 683, 990
Marigo, P., & Girardi, L. 2007, ASP Conference Series, 374, 33 (MG07)
Menzies, J. W., Feast, M. W., & Whitelock, P. A. 2006, MNRAS, 369, 783
Miller, G. E., & Scalo, J. M. 1979, ApJS, 41, 513
Olivier, E. A., Whitelock, P., & Marang, F. 2001, MNRAS, 326, 490
Ostlie, D. A., & Cox, A. N. 1986, ApJ, 311, 864
Percy, R. J. 1997, The Journal of the American Association of Variable Star Observers, 25, 93
Reimers, D. 1975, Mem. Soc. R. Sci. Liege, 8, 369
Renzini, A., & Voli, M. 1981, A&A, 94, 175
Stancliffe, R. J., & Jeffery, C. S. 2007, MNRAS, 375, 1280
van Leeuwen, F., Feast, M. W., Whitelock, P. A., & Yudin, B. 1997, MNRAS, 287, 955
Vassiliadis, E., & Wood, P. R. 1993, ApJ, 413, 641
Wagenhuber, J., & Groenewegen, M. A. T. 1998, A&A, 340, 183
Whitelock, P. A., Marang, F., & Feast, M. 2000, MNRAS, 319, 728
Willson, L. A. 2007, ASP Conference Series, 378, 211
Wood, P. R. 1990, ASP Conference Series, 11, 355
Wood, P. R., & Cahn, J. H. 1977, ApJ, 211, 499
Wood, P. R., & Sebo, K. M. 1996, MNRAS, 282, 958
Yungelson, L., & Tutukov, A. V. 1993, International Astronomical Union. Symposium, 155, 389
Zhu, C. H., Lü, G. L., Wang, Z. J., & Zhang, J. 2008, Chinese Physics B, 17, 1518
Zhu, C. H., & Zha, C. Z. 2005, ChJAA (Chin. J. Astron. Astrophys.), 5, 419